



Numerical Study of MHD Natural Convection in Trapezoidal Enclosure Filled With (50%MgO-50%Ag/Water) Hybrid Nanofluid: Heated Sinusoidal from Below

Mohammed Azeez Alomari¹, Khaled Al-Farhany^{1*}, Alaa Liaq Hashem¹, Mohamed F. Al-Dawody¹, Fares Redouane², Olalekan Adebayo Olayemi³

¹ Department of Mechanical Engineering, University of Al-Qadisiyah, Al-Qadisiyah 58001, Iraq

² LGIDD, Ahmed ZABANA University, Relizane 48000, Algeria

³ Department of Aeronautics and Astronautics, Faculty of Engineering and Technology, Kwara State University, Malete 241104, Nigeria

Corresponding Author Email: Khaled.alfarhany@qu.edu.iq

<https://doi.org/10.18280/ijht.390425>

ABSTRACT

Received: 26 April 2021

Accepted: 7 June 2021

Keywords:

hybrid nanofluid, MHD, non-uniform heat, trapezoidal cavity

Numerical simulation of MHD free convection in a two-dimensional trapezoidal cavity of a hybrid nanofluid has been carried out in this research. The cavity is heated sinusoidal from the bottom wall, and the inclined walls are cooled while the top wall is isolated. The hybrid nanofluid (MgO-Ag/water) has been used as a working fluid. The numerical simulation has been validated with past papers and met a good agreement. The considered parameters are a range of Rayleigh number ($Ra = 10^3$ to 10^6), Hartmann number ($Ha = 0$ to 60) and volume fraction ($\phi = 0$ to 0.02). The results are presented as isotherms, stream functions, local and average Nusselt numbers, from which it is observed that the strength of the stream functions and isotherms increases with the increase of the Ra and ϕ while the increase in Hartmann number reduce the circulation of the flow and increases the isotherms strength. Also, the Nusselt number is increases with Ra and ϕ while it decreases with Ha .

1. INTRODUCTION

Free, natural, convection is a popular phenomenon in many applications in which the fluid flow is controlled by bouncy without applying any external forces. Natural convection in the closed enclosure has attracted many researchers, who apply an extensive study to modify the possibility of heat transfer manipulation because it plays a major role in many engineering applications such as cooling systems of chips and microelectronic devices, reactors, geothermal systems, and solar collectors [1-7].

The shapes of the closed enclosures, in which free convection is a dominant force, are different depending on the type of the application, and this reason behind testing a wide difference shape. Some considered enclosures are uniform such as square, triangular, trapezoidal, rhombic, parallelogrammatical, etc. while others are non-uniform, complex, shapes [8-13]. Free convection in a trapezoidal cavity with a top wall that is wider than the bottom wall and is filled with porous material was numerically studied by Basak et al. [14]. The cavity is heated from the bottom wall and cooled by the vertical walls while the top wall is maintained isolation. The inclination angle of the trapezoid is varying from ($\phi = 0^\circ$) for a square shape to ($\phi = 45^\circ$), for a trapezoidal shape. Furthermore, Ra and Pr numbers have been considered to be varying from (10^3 to 10^6) and from (0.026 to 988.24) respectively. They stated that the heat transfer and circulation strength increase with the increase of ϕ , Pr , and Ra . These results have been confirmed by Mehryan et al. [15] who added that the strength of heat and flow circulation are higher in the square cavity than in trapezoidal when the top wall length is shorter than the bottom. Venkatadri et al. [16] numerically

investigated free convection of air in a closed trapezoidal enclosure where the top wall is inclined while the other walls are vertical on the left and right sides, and horizontal on the bottom. The authors investigated the effect of applying a range of Rayleigh number (Ra) and thermal radiation (Rd) on free convection where ($Ra = 10^3$ to 10^6) and ($Rd = 1$ to 5). The results showed that the transfer intensive of heat and the strength of circulation increase with the increase of Ra and Rd . Rao and Barman [17] studied natural convection in a square porous cavity in which the right wall, which represents the cold side, is away from the wall while others are straight and adiabatic except part of the left wall which contains the heat source. They considered a range of Ra (10 to 10^3), the ratio of the heater length to the right wall length, ε , (0.25 to 1), and the amplitude of the wavy wall, a , (0.05 to 0.25). The results stated that the strength of convection increases with the increase of the Ra number and decreases with the rise of ε , which is the effect recognized at high Ra . Also, the increase of the amplitude of the wavy wall increases the roughness of the wall and hence increases the convection strength.

In order to increase the heat transfer capability, the authors found that adding nanoparticles to the working fluid can achieve that goal [18-22]. Mahalakshmi et al. [23] studied free convection in a rectangular enclosure filled with nanofluid and contains two heat sources positioned at the bottom wall as well as the center of the cavity. The authors considered three types of nanoparticles (Ag, CuO, and Al_2O_3) with a range of volume fraction ($\phi = 0, 0.03, 0.06, \text{ and } 0.09$), Ra ($10^3, 10^6, 10^7$), and the length of the central heater ($0.25, 0.5, 0.75$). From the results, they stated that the enhancement of heat increased by adding nanoparticles, and the strength of the enhancement increases with the increase of the volume fraction, Ra , and the heater

length. Also, the best nanofluid of the three tested types was the Ag-water. Naseri Nia et al. [24] studied free convection of nanofluid in L- cavity with a single baffle. The results confirmed the previous statement, where they found that heat transfer enhances by adding nanoparticles to the main fluid and enhances further increases with the increase of the volume fraction. Furthermore, the baffle remarkably enhances the transfer of heat which increases with the increase of the baffle length.

The researcher used different types of nanoparticles (metals, carbon material, etc.) in order to understand their effect on fluid flow and heat transfer enhancement. After that, they started to use more than one combination of nanoparticles with the main fluid which is called “hybrid nanofluids” where these types of nanofluids are more effective in rising heat transfer [25-28]. Mohebbi et al. [29] investigated free convection in T-cavity filled with hybrid fluid and part of it filled with porous media. Their results presented that the heat transfer increases with the increase of the Ra number and the volume fraction of the nanofluid. Tayebi et al. [30] studied free convection in an annular enclosure with an elliptical source of heat, absorption, or generation, and filled with (Cu-Al₂O₃/water) hybrid nanofluid. They found that the entropy generation as well as the Nusselt number increase with the increase of the Ra number and the concentration of the nanoparticles.

Applying magnetohydrodynamic field can affect the heat transfer enhancement as well as the strength of the vortices, for that reason an extensive study has been done to understand the role of the MHD [31-35]. Free convection of a (CuO-H₂O/water) nanofluid in a three-dimensional trapezoidal cavity with a corrugated bottom wall under the magnetic effect has been studied by Selimefendigil and Öztöp [36]. They used a range of Ra and Ha numbers (Ra=10⁴ to 10⁶ and Ha= 0 to 40), volume fraction ($\phi= 0$ to 0.04), and the number of triangles of the bottom wall (N= 0 to 16). They found that the value of Nu_L and Nu_{avg} increase with the increase of Ra, N, and ϕ while reduced when applying the MHD force. Furthermore, these reductions in heat transfer increase with the increase of the Ha number.

The novelty of the current work is to study the effect of applying different strengths of magnetic field on the free convection in a closed trapezoidal-shaped enclosure filled with (50%MgO-50%Ag/ Water) hybrid nanofluid and heated using a sinusoidal heater source from the bottom and cooled by the two inclined walls.

2. MATHEMATICAL MODELING

To solve the considered problem, a FEM is employed. The problem sketch with the applied boundary condition can be seen in Figure 1. A trapezoidal enclosure is heated sinusoidal from the bottom and cooled by the two inclined side walls while the top wall is treated as adiabatically isolated. The closed cavity is to be filled with hybrid nanofluid (50%MgO-50%Ag/ Water) for which the properties are mentioned in Table 1. The cavity is located under the magnetohydrodynamic effect. The current study considered some variables that can affect the flow behavior and transfer of heat such as the Ha, Ra, and ϕ . The simulation depends on the assumption below:

1. The hybrid nanofluid is assumed to be in single-phase and thermal equilibrium.

2. The main fluid (water) and the nanofluid are homogeneous so there is no slip for the particles.

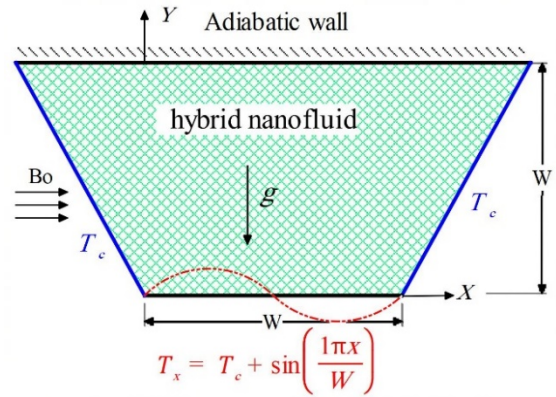


Figure 1. Physical geometry of the model

Table 1. Thermophysical properties of the fluid and nanoparticles [37, 38]

| Properties | Pure water | MgO | Ag |
|------------------------------|-----------------------|-----------------------|----------------------|
| C_p (J/kg K) | 4179 | 879 | 235 |
| ρ (kg/m ³) | 997.1 | 3580 | 10500 |
| α (m ² /s) | 1.47x10 ⁻⁷ | 95.3x10 ⁻⁷ | 174x10 ⁻³ |
| k (W/m.K) | 0.613 | 30 | 429 |
| β (1/K) | 21x10 ⁻⁵ | 33.6x10 ⁻⁶ | 5.4x10 ⁻⁵ |
| μ (kg/m.s) | 8.9x10 ⁻⁴ | - | - |

The governing equations for the problem are as follows, based on the above assumptions [37]:

$$\frac{\partial u}{\partial x} + \frac{\partial v}{\partial y} = 0 \quad (1)$$

$$\left(u \frac{\partial u}{\partial x} + v \frac{\partial u}{\partial y}\right) = -\frac{1}{\rho_{hnf}} \frac{\partial p}{\partial x} + \frac{\mu_{hnf}}{\rho_{hnf}} \left(\frac{\partial^2 u}{\partial x^2} + \frac{\partial^2 u}{\partial y^2}\right) \quad (2)$$

$$\left(u \frac{\partial v}{\partial x} + v \frac{\partial v}{\partial y}\right) = -\frac{1}{\rho_{hnf}} \frac{\partial p}{\partial y} + \frac{\mu_{hnf}}{\rho_{hnf}} \left(\frac{\partial^2 v}{\partial x^2} + \frac{\partial^2 v}{\partial y^2}\right) + \frac{(\rho\beta)_{hnf}}{\rho_{hnf}} g(T - T_c) - \frac{\sigma_{hnf} B_o^2}{\rho_{hnf}} v \quad (3)$$

$$u \frac{\partial T}{\partial x} + v \frac{\partial T}{\partial y} = \frac{k_{hnf}}{(\rho C_p)_{hnf}} \left(\frac{\partial^2 T}{\partial x^2} + \frac{\partial^2 T}{\partial y^2}\right) \quad (4)$$

The non-dimensional form of the governing equations is obtained using the non-dimensional parameters mentioned below [37]:

$$X = \frac{x}{W}, Y = \frac{y}{W}, U = \frac{uW}{\alpha_f}, V = \frac{vW}{\alpha_f}, \theta = \frac{T-T_c}{(T_h-T_c)}, P = \frac{pW^2}{\rho_f \alpha_f^2} \quad (5)$$

The following non-dimensional numbers were used:

$$Ra = \frac{g\beta_f(T_h-T_c)W^3}{\nu_f \alpha_f}, Pr = \frac{\nu_f}{\alpha_f}, Da = \frac{K}{W^2}, Ha = B_o W \sqrt{\frac{\sigma_{hnf}}{\rho_f \nu_f}}, \alpha_f = \frac{k_f}{(\rho C_p)_f} \quad (6)$$

The Eqns. (1) to (4) are formulated in the following dimensionless equations:

$$\frac{\partial U}{\partial X} + \frac{\partial V}{\partial Y} = 0 \quad (7)$$

The momentum equation is given by [37]:

$$\begin{aligned} & \frac{\rho_{hnf}}{\rho_f} \left(U \frac{\partial U}{\partial X} + V \frac{\partial U}{\partial Y} \right) \\ &= - \frac{\partial P}{\partial X} + \frac{\mu_{hnf}}{\mu_f} Pr \left(\frac{\partial^2 U}{\partial X^2} + \frac{\partial^2 U}{\partial Y^2} \right) \end{aligned} \quad (8)$$

$$\begin{aligned} & \frac{\rho_{hnf}}{\rho_f} \left(U \frac{\partial V}{\partial X} + V \frac{\partial V}{\partial Y} \right) \\ &= - \frac{\partial P}{\partial Y} + \frac{\mu_{hnf}}{\mu_f} Pr \left(\frac{\partial^2 V}{\partial X^2} + \frac{\partial^2 V}{\partial Y^2} \right) \\ &+ \frac{(\rho\beta)_{hnf}}{(\rho\beta)_f} Ra \cdot Pr \cdot \theta - Ha^2 \\ &\cdot Pr \cdot V \end{aligned} \quad (9)$$

The energy equation is given by:

$$U \frac{\partial \theta}{\partial X} + V \frac{\partial \theta}{\partial Y} = \frac{\alpha_{hnf}}{\alpha_f} \left(\frac{\partial^2 \theta}{\partial X^2} + \frac{\partial^2 \theta}{\partial Y^2} \right) \quad (10)$$

The density, thermal diffusivity, thermal expansion coefficient, and heat capacitance of hybrid nanofluids are set to the following values [37, 39]:

$$\alpha_{hnf} = \frac{k_{hnf}}{(\rho C_p)_{hnf}} \quad (11)$$

$$\phi = \phi_{Ag} + \phi_{MgO} \quad (12)$$

$$\rho_{hnf} = (1 - \phi)\rho_f + (\phi_{Ag} \cdot \rho_{Ag} + \phi_{MgO} \cdot \rho_{MgO}) \quad [40] \quad (13)$$

$$\begin{aligned} (\rho C_p)_{hnf} &= (1 - \phi)(\rho C_p)_f \\ &+ (\phi_{Ag} \cdot (\rho C_p)_{Ag} \\ &+ \phi_{MgO} \cdot (\rho C_p)_{MgO}) \end{aligned} \quad (14)$$

$$\begin{aligned} (\rho\beta)_{hnf} &= (1 - \phi)(\rho\beta)_f \\ &+ (\phi_{Ag} \cdot (\rho\beta)_{Ag} \\ &+ \phi_{MgO} \cdot (\rho\beta)_{MgO}) \end{aligned} \quad (15)$$

Regarding hybrid nanofluid viscosity, it can be obtained from the experimental study of Refs. [37, 38].

$$\begin{aligned} \frac{\mu_{hnf}}{\mu_f} &= (1 + 32.795\phi) - 7214\phi^2 + 714600\phi^3 \\ &- 0.1941 \times 10^8 \phi^4 \end{aligned} \quad (16)$$

for $0 \leq \phi \leq 0.02$,

Regarding nanofluid thermal conductivity, it is given by [37, 38]:

$$\begin{aligned} & \frac{k_{hnf}}{k_f} \\ &= \frac{0.1747 \times 10^5 + \phi}{0.1747 \times 10^5 - 0.1498} \\ &\times 10^6 \phi + 0.1117 \times 10^7 \phi^2 + 0.1997 \times 10^8 \phi^3 \end{aligned} \quad (17)$$

for $0 \leq \phi \leq 0.03$,

$$\frac{\sigma_{hnf}}{\sigma_f} = 1 + \frac{3(\sigma_{hnf} - \sigma_f)\phi}{(\sigma_{hnf} + 2\sigma_f) - (\sigma_{hnf} - \sigma_f)\phi} \quad (18)$$

2.1 Stream function

The flow fields within the cavity are represented by streamline contours, and they, therefore, be presented in the following format:

$$U = \frac{\partial \psi}{\partial Y}, V = - \frac{\partial \psi}{\partial X} \quad (19)$$

The stream function in dimensionless approximation equation is given by:

$$\frac{\partial^2 \psi}{\partial X^2} + \frac{\partial^2 \psi}{\partial Y^2} = \frac{\partial U}{\partial Y} - \frac{\partial V}{\partial X} \quad (20)$$

2.2 Local nusselt number

The average and local Nusselt numbers described by [37, 41] have been used to investigate the effects of various parameters on heat transfer:

$$Nu_L = - \left(\frac{k_{hnf}}{k_f} \right) \frac{\partial \theta}{\partial Y} \quad (21)$$

$$Nu = \int_0^1 Nu_L dX \quad (22)$$

2.3 Initial boundary conditions

The following boundary conditions were used to figure out the two dimensionless equations in this study.

At the bottom hot wall of the trapezoidal:

$$T_x = T_c + \text{Sin}\left(\frac{\pi x}{W}\right), U = V = 0$$

At the inclined walls of the trapezoidal:

$$\theta = U = V = 0$$

At the insulation walls of the trapezoidal:

$$\frac{\partial \theta}{\partial Y} = U = V = 0$$

2.4 Solution procedure

The present work has been solved by applying the FEM. These equations are contained nonlinear factors in the momentum and energy equations, to simplify these equations the under-relaxation factor is applied. The solution will converge if the error of the equations' variables satisfies the following criteria.

$$\left| \frac{\Gamma^{i+1} - \Gamma^i}{\Gamma^{i+1}} \right| \leq \eta \quad (23)$$

i: is the iteration number.

Γ : is a sample for all variables such as temperature, pressure,

velocity in x and y directions.

η : is the convergence criterion which is set to be 10^5 in this study.

Furthermore, it is known that the increase of the cell numbers will increase the accuracy of the results; however, a very high refine mesh means a long time and high requirements for that reason it is important to have a mesh independence test. This test determines the minimum number of cells that give an acceptable accuracy. For the current research, the independence test has been done as can be seen in Table 2 while the mesh sample is shown in Figure 2. The mesh size (9277) has been selected for all cases in this study.

Table 2. The relation between the average Nusselt number along the bottom wall and the number of elements used for $Ra = 10^6$, $\phi=0.02$, and $Ha=0$

| Mesh size | Average Nusselt number | Error |
|-------------|------------------------|-------|
| 737 | 13.615 | --- |
| 1354 | 13.401 | 1.57 |
| 2072 | 13.408 | 0.05 |
| 3582 | 13.367 | 0.3 |
| 9277 | 13.328 | 0.29 |
| 23353 | 13.316 | 0.09 |

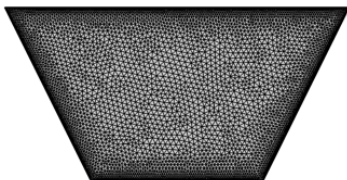
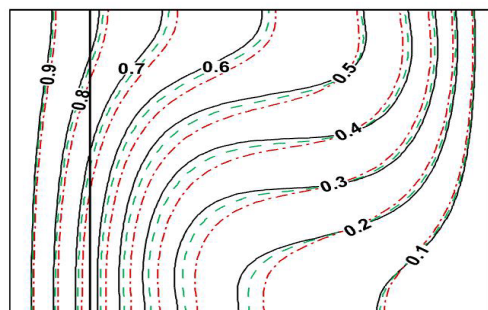
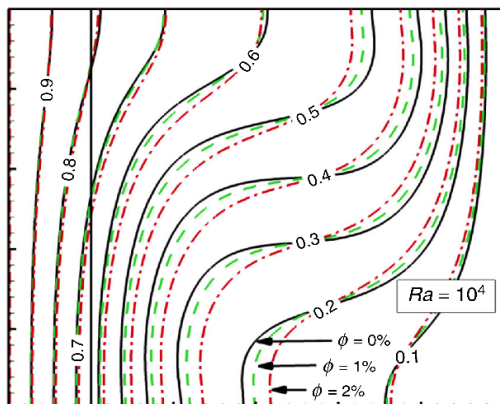


Figure 2. The triangle mesh distribution of the enclosure



Present work



Ghalambaz et al.

Figure 3. Comparison between the present study and Ghalambaz et al. [37] for isothermal contours of hybrid nanofluent Ag–MgO/water at $Ra = 10^4$ for $Rk=1$

2.5 Model validation

To assess the current code it is crucially important to be validated with past published papers for this reason a comparison has been done with Ghalambaz et al. [37] for square cavities that are filled with hybrid nanofluent (Figure 3). The results met a high agreement with a very low percentage error.

3. RESULTS AND DISCUSSION

Free convection of a hybrid nanofluent in a trapezoidal cavity under the magnetohydrodynamic effect has been studied numerically. The cavity is heated from the bottom with a non-uniform heat source. The circulation of the fluid inside the trapezoidal cavity is driven due to the force of the buoyancy without any external force and is hence called natural convection. The hybrid nanofluent that has been considered in this study is MgO-Ag/H₂O Hybrid nanofluent. The considered parameters in the present work are a range of volume fraction ($\phi=0, 0.01, 0.02$), Ra number ($Ra= 10^3, 10^4, 10^6$) and Ha number ($Ha= 0, 10, 15, 30, 60$). The outcomes of the present results are demonstrated as contours for stream functions and isotherms lines as well as the local and average Nusselt number.

Figure 4 explains the effect of Ra on the stream functions and isotherms lines at fixed values of the Ha number ($Ha=20$) and Volume fraction ($\phi= 0.02$). At low Ra number ($Ra= 10^3$), the cavity generates two large vortices that are equal in strength and size and different in the orientation, where one of them flows clockwise and the other flows anti-clockwise. As the Ra number increases ($Ra=10^4$), the strength of the flow enhances from ($\Psi_{max}=0.068$) to ($\Psi_{max}=0.86$) then the stream function strength is further increasing with further increase in Ra number ($Ra=10^6$) to be ($\Psi_{max}=21$). From the right side of the figure which presents the isotherms contour, it is clear that the isotherm enhances with the increase of the Ra number which means an increase in the convection force.

Figure 5 presents the effect of applying different strengths of magnetic fields ($Ha= 0, 10, 30, 60$) at constant Ra number ($Ra=10^6$) and volume fraction ($\phi= 0.02$). For the streams, the strength of the circulation decreases with the increase of the Ha number from ($\Psi_{max}=38$) at ($Ha= 0$) to ($\Psi_{max}= 9.6$) at ($Ha=60$). On the other hand, the strength of the isotherms increases with the increase of the Ha number, and the physical explanation is due to have both forces, buoyancy and magnetic, in one direction and hence enhances the isotherms.

Figure 6 demonstrates the effect of applying different volume fractions ($\phi=0, 0.01, 0.02$) at constant Ra and Ha numbers ($Ra=10^5$ and $Ha= 40$). The streams and isotherms' strength increases with the increase of the volume fraction.

Local Nusselt number presents the ratio of the convection to the conduction of the heat transfer. Figure 7 presents the variation of the local Nusselt number, along the hot wall, with different values of the Ra number at constant Ha number and volume fraction. It is clear that the value of the local Nusselt number increases with the increase of the Ra number and hence the convection inside the cavity increases with the increase of the Ra number. Figure 8 presents the variation of the local Nusselt number at different Ha numbers and constant Ra and ϕ . The figure shows that the Nu_L decreases with the increase of the Ha number which means that the magnetic field enhances the conduction and decreases the convection inside

the cavity. Figure 9 presents the variation of the Nu_L with different values of volume fraction ($\phi = 0, 0.01, 0.02$) at constant Ra and Ha numbers.

Figure 10 presents the variation of the Nu_{avg} number at different values of Ra number, volume fraction, and Ha

number. From the figure, it is noticeable that the value Nu_{avg} increases with the increase of the Ra number and the volume fraction while the magnetic field enhances acts negatively on the Nu_{avg} .

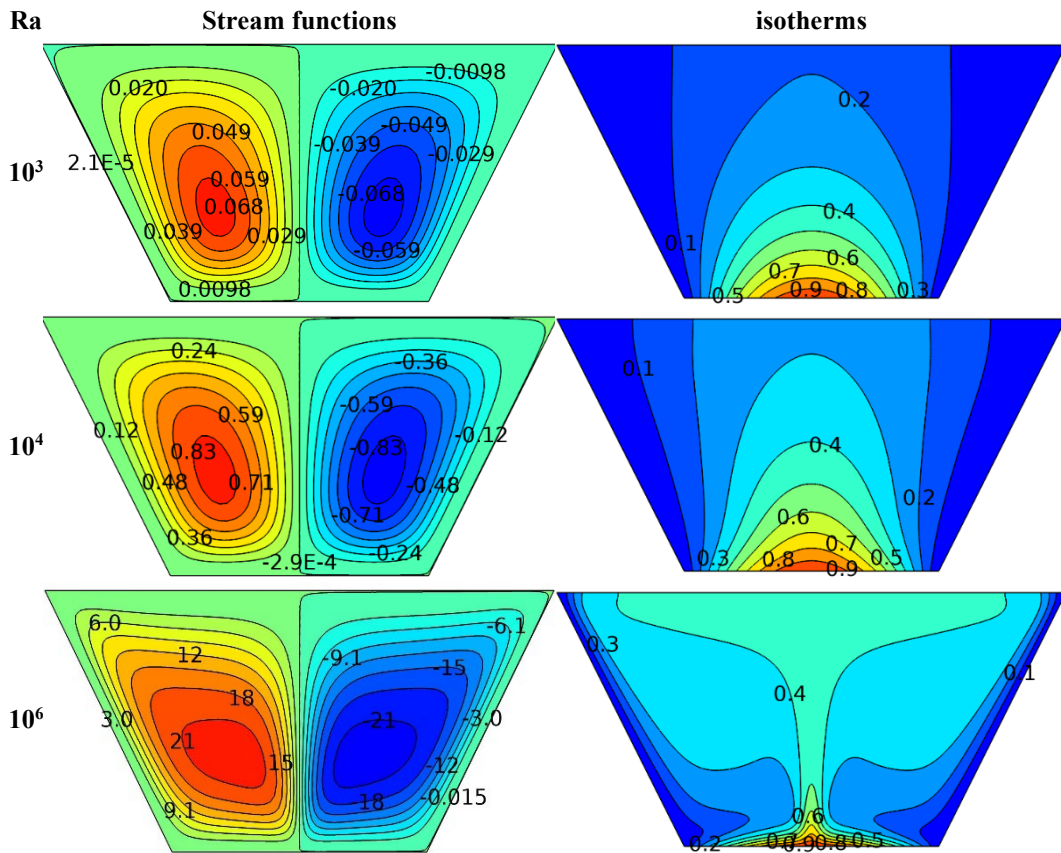
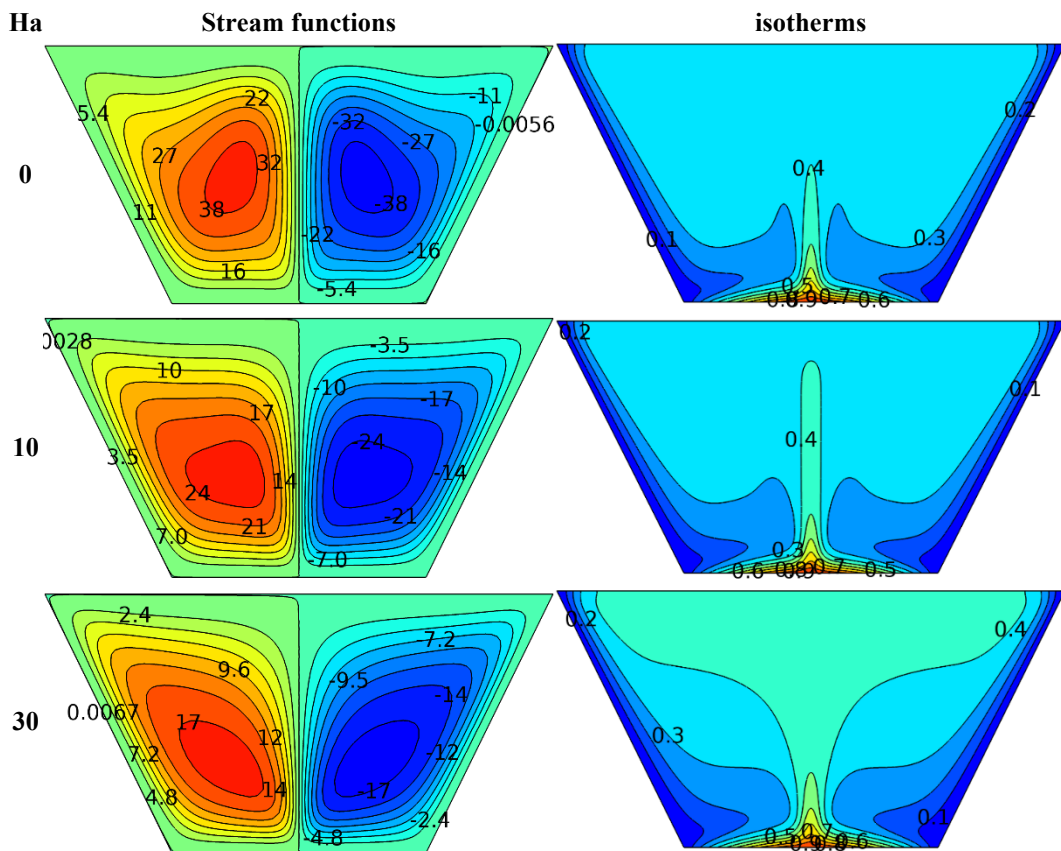


Figure 4. Visualization of stream functions and isotherms with Rayleigh number at $Ha = 20$ and $\phi = 0.02$



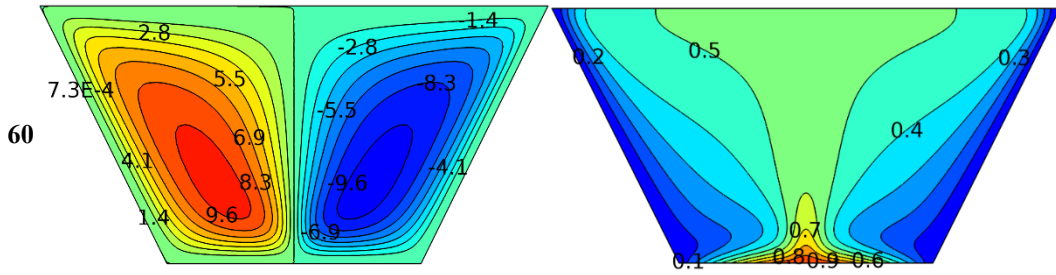


Figure 5. Visualization of stream functions and isotherms with Hartmann number at $Ra = 10^6$ and $\phi = 0.02$

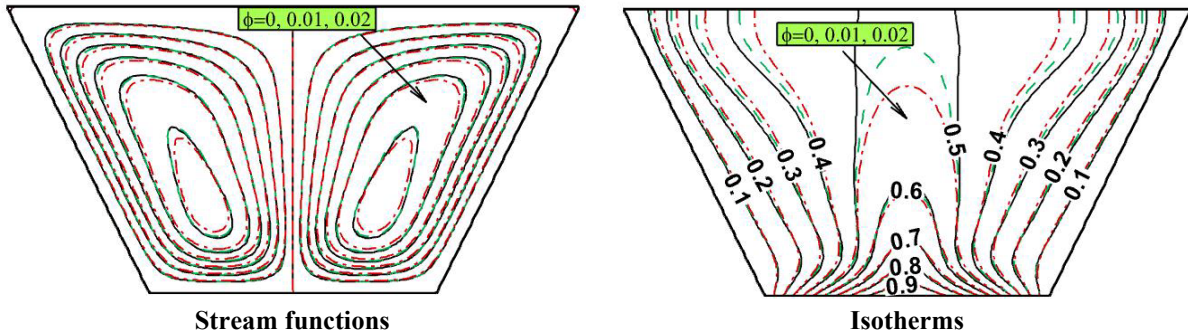


Figure 6. Visualization of stream functions and isotherms with volume fraction at $Ra = 10^5$ and $Ha = 40$

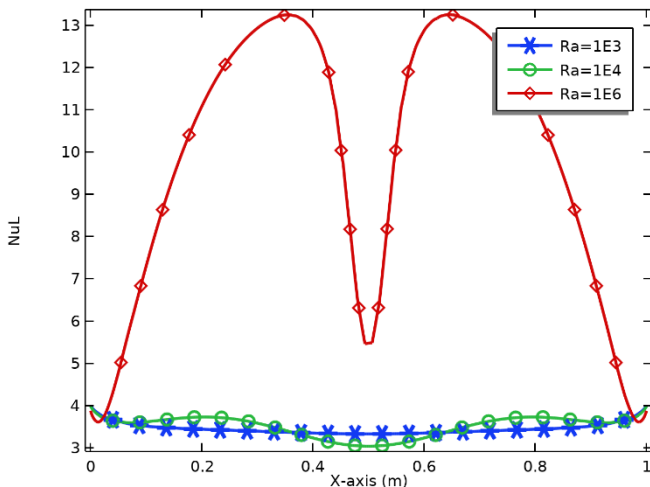


Figure 7. Local Nusselt number (Nu_L) along the bottom wall at various Rayleigh numbers (Ra) for $Ha=20$ and $\phi = 0.02$

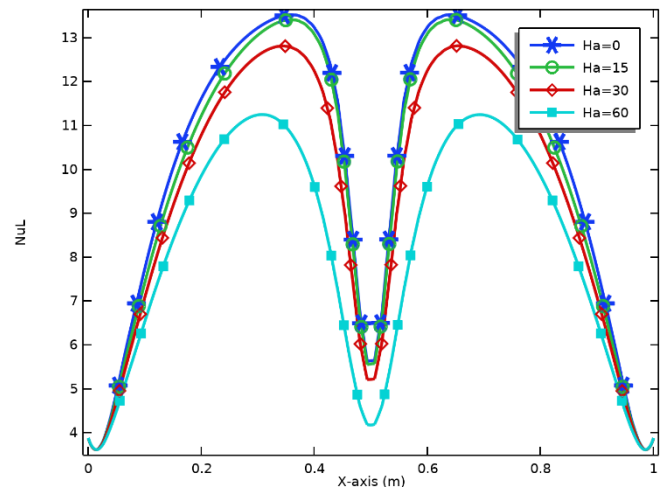


Figure 8. Local Nusselt number (Nu_L) along the bottom wall at various Hartmann numbers at $Ra = 10^6$ and $\phi = 0.02$

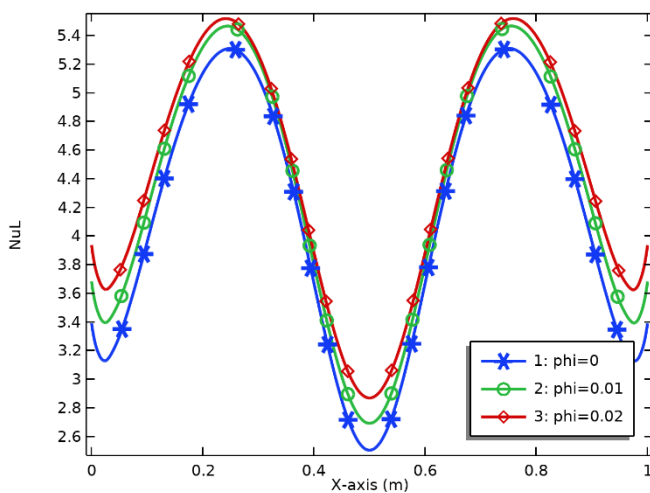


Figure 9. Local Nusselt number (Nu_L) along the bottom wall at various volume fractions at $Ra = 10^5$ and $Ha = 40$

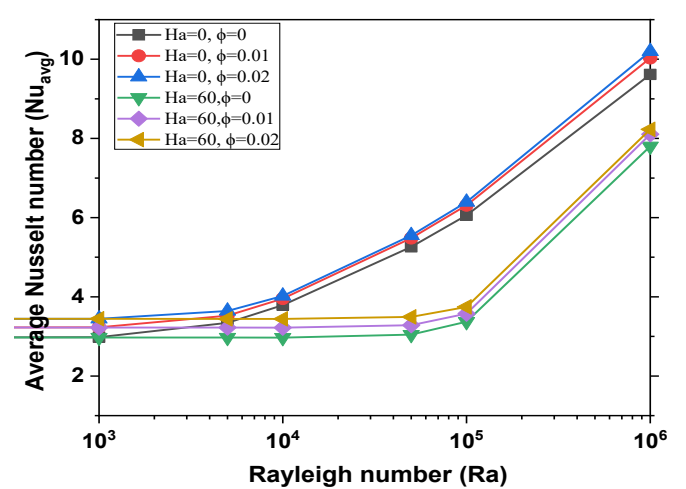


Figure 10. Average Nusselt number (Nu_{avg}) of the bottom wall at various volume fractions, Ra and Ha

4. CONCLUSION

The effect of the MHD and hybrid nanofluid on the natural convection in a closed enclosure, trapezoidal shape, has been investigated in this paper. The main results can be concluded as:

- The circulation of the hybrid nanofluid inside the cavity increases with the increase of the Ra number where it increases from $\Psi_{\max} = 0.068$ at $Ra=10^6$ to $\Psi_{\max} = 21$ at $Ra= 10^6$ and these numbers at $Ha = 20$. Furthermore, the value of Ψ_{\max} is much higher at free MHD where $\Psi_{\max} = 38$ at $Ra=10^6$ while it further decreases at the high presence of MHD to be $\Psi_{\max} = 9.6$ at $Ha= 60$. Also, the strength of the streams barely increases with the increase of the volume fraction.
- The isotherms enhance with the increase of the Rayleigh number at constant Hartman number to be very strong at higher Ra number. Also, at constant Rayleigh number, the streams seem to be increased with the increase of the Hartman number. Furthermore, the effect of the volume fraction has a small effect on the streams where it enhances with the increase of the volume fraction.
- The Nu_L and Nu_{avg} are increasing with the increase of the Rayleigh number and volume fraction while decreasing with the increase of the Hartman number.

REFERENCES

- [1] Abbasi-Shavazi, E., Torres, J.F., Hughes, G., Pye, J. (2020). Experimental correlation of natural convection losses from a scale-model solar cavity receiver with non-isothermal surface temperature distribution. *Solar Energy*, 198: 355-375. <https://doi.org/10.1016/j.solener.2020.01.023>
- [2] Saha, L.K., Bala, S.K., Roy, N.C. (2020). Natural convection of dusty nanofluids within a concentric annulus. *The European Physical Journal Plus*, 135(9): 732. <https://doi.org/10.1140/epjp/s13360-020-00759-0>
- [3] Miao, G., Zhang, L., Zhang, J., Ge, S., Xia, N., Qian, S., Yu, D., Qiu, X. (2020). Free convective PCR: From principle study to commercial applications-A critical review. *Anal Chim Acta*, 1108: 177-197. <https://doi.org/10.1016/j.aca.2020.01.069>
- [4] Mugi, V.R., Chandramohan, V.P. (2021). Energy and exergy analysis of forced and natural convection indirect solar dryers: Estimation of exergy inflow, outflow, losses, exergy efficiencies and sustainability indicators from drying experiments. *Journal of Cleaner Production*, 282: 124421. <https://doi.org/10.1016/j.jclepro.2020.124421>
- [5] Soboleva, E.B. (2018). Density-driven convection in an inhomogeneous geothermal reservoir. *International Journal of Heat and Mass Transfer*, 127: 784-798. <https://doi.org/10.1016/j.ijheatmasstransfer.2018.08.019>
- [6] Zhang, C., Shi, S., Lu, Y., Qiang, Y., Wu, Y., Ma, C. (2020). Heat discharging and natural convection heat transfer performance of coil heat exchanger in single molten salt tank. *Applied Thermal Engineering*, 166: 114689. <https://doi.org/10.1016/j.applthermaleng.2019.114689>
- [7] Al-Farhany, K., Al-Dawody, M.F., Hamzah, D.A., Hamza, N.H. (2020). Numerical study of nanofluid natural convection in a partially heated tall enclosure. *IOP Conference Series: Materials Science and Engineering*, 928: 022137. <https://doi.org/10.1088/1757-899x/928/2/022137>
- [8] Biswal, P., Basak, T. (2017). Entropy generation vs energy efficiency for natural convection based energy flow in enclosures and various applications: A review. *Renewable and Sustainable Energy Reviews*, 80: 1412-1457. <https://doi.org/10.1016/j.rser.2017.04.070>
- [9] Das, D., Roy, M., Basak T. (2017). Studies on natural convection within enclosures of various (non-square) shapes – A review. *International Journal of Heat and Mass Transfer*, 106: 356-406. <https://doi.org/10.1016/j.ijheatmasstransfer.2016.08.034>
- [10] Izadi, S., Armaghani, T., Ghasemiasl, R., Chamkha, A.J., Molana, M. (2019). A comprehensive review on mixed convection of nanofluids in various shapes of enclosures. *Powder Technology*, 343: 880-907. <https://doi.org/10.1016/j.powtec.2018.11.006>
- [11] Tao, W.Q., He Y.L., Chen, L. (2019). A comprehensive review and comparison on heatline concept and field synergy principle. *International Journal of Heat and Mass Transfer*, 135: 436-459. <https://doi.org/10.1016/j.ijheatmasstransfer.2019.01.143>
- [12] Al-Farhany, K., Abdulsahib, A.D. (2021). Study of mixed convection in two layers of saturated porous medium and nanofluid with rotating circular cylinder. *Progress in Nuclear Energy*, 135: 103723. <https://doi.org/10.1016/j.pnucene.2021.103723>
- [13] Olayemi, O.A., Al-Farhany, K., Temitope, O.J., Victor, O.O., Odetunde, C.B., Adegun, I.K. (2021). Parametric study of natural convection heat transfer from an inclined rectangular cylinder embedded in a square enclosure. *Australian Journal of Mechanical Engineering*. <https://doi.org/10.1080/14484846.2021.1913853>
- [14] Basak, T., Roy, S., Singh, A., Balakrishnan, A.R. (2009). Natural convection flows in porous trapezoidal enclosures with various inclination angles. *International Journal of Heat and Mass Transfer*, 52(19-20): 4612-4623. <https://doi.org/10.1016/j.ijheatmasstransfer.2009.01.050>
- [15] Mehryan, S.A.M., Ghalambaz, M., Kalantar, Feeoj, R., Hajjar, A., Izadi, M. (2020). Free convection in a trapezoidal enclosure divided by a flexible partition. *International Journal of Heat and Mass Transfer*, 149: 119186. <https://doi.org/10.1016/j.ijheatmasstransfer.2019.119186>
- [16] Venkatadri, K., Anwar Bég, O., Rajarajeswari P., Ramachandra Prasad, V. (2020). Numerical simulation of thermal radiation influence on natural convection in a trapezoidal enclosure: Heat flow visualization through energy flux vectors. *International Journal of Mechanical Sciences*, 171: 105391. <https://doi.org/10.1016/j.ijmecsci.2019.105391>
- [17] Rao, P.S., Barman, P. (2021). Natural convection in a wavy porous cavity subjected to a partial heat source. *International Communications in Heat and Mass Transfer*, 120: 105007. <https://doi.org/10.1016/j.icheatmasstransfer.2020.105007>
- [18] Armaghani, T., Kasaeipoor, A., Alavi, N., Rashidi, M.M. (2016). Numerical investigation of water-alumina nanofluid natural convection heat transfer and entropy generation in a baffled L-shaped cavity. *Journal of Molecular Liquids*, 223: 243-251.

- <https://doi.org/10.1016/j.molliq.2016.07.103>.
- [19] Sheremet, M.A., Revnic, C., Pop, I. (2017). Natural convective heat transfer through two entrapped triangular cavities filled with a nanofluid: Buongiorno's mathematical model. *International Journal of Mechanical Sciences*, 133: 484-494. <https://doi.org/10.1016/j.ijmecsci.2017.09.010>
- [20] Uddin, M., Rahman, M. (2020). Heat transportation in copper oxide-water nanofluid filled triangular cavities. *International Journal of Heat and Technology*, 38(1): 106-124. <https://doi.org/10.18280/ijht.380112>
- [21] Azizul, F.M., Alsabery, A.I., Hashim, I., Chamkha, A.J. (2021). Impact of heat source on combined convection flow inside wavy-walled cavity filled with nanofluids via heatline concept. *Applied Mathematics and Computation*, 393: 12574. <https://doi.org/10.1016/j.amc.2020.125754>
- [22] Shi, L., He, Y.R., Hu, Y.W., Wang, X.Z. (2019). Controllable natural convection in a rectangular enclosure filled with $\text{Fe}_3\text{O}_4/\text{CNT}$ nanofluids. *International Journal of Heat and Mass Transfer*, 140: 399-409. <https://doi.org/10.1016/j.ijheatmasstransfer.2019.05.104>
- [23] Mahalakshmi, T., Nithyadevi, N.F., Oztop H., Abu-Hamdeh, N. (2018). Natural convective heat transfer of Ag-water nanofluid flow inside enclosure with center heater and bottom heat source. *Chinese Journal of Physics*, 56(4): 1497-1507. <https://doi.org/10.1016/j.cjph.2018.06.006>
- [24] Naseri Nia, S., Rabiei, F., Rashidi, M.M., Kwang, T.M. (2020). Lattice Boltzmann simulation of natural convection heat transfer of a nanofluid in a L-shape enclosure with a baffle. *Results in Physics*, 19: 103413. <https://doi.org/10.1016/j.rinp.2020.103413>
- [25] Babar, H., Ali, H.M. (2019). Towards hybrid nanofluids: Preparation, thermophysical properties, applications, and challenges. *Journal of Molecular Liquids*, 281: 598-633. <https://doi.org/10.1016/j.molliq.2019.02.102>
- [26] Izadi, M., Sheremet, M.A., Mehryan, S.A.M. (2020). Natural convection of a hybrid nanofluid affected by an inclined periodic magnetic field within a porous medium. *Chinese Journal of Physics*, 65: 447-458. <https://doi.org/10.1016/j.cjph.2020.03.006>
- [27] Jasim, H. (2020). Enhancement of natural convection heat transfer of hybrid design heat sink. *International Journal of Heat and Technology*, 38(1): 165-170. <https://doi.org/10.18280/ijht.380118>
- [28] Abdulsahib, A.D., Al-Farhany, K. (2020). Numerical investigation of the nanofluid mixed convection on two layers enclosure with rotating cylinder: High Darcy number effects. *2020 IOP Conf. Ser.: Mater. Sci. Eng.*, 928: 022001. <https://doi.org/10.1088/1757-899X/928/2/022001>
- [29] Mohebbi, R., Mehryan, S.A.M., Izadi, M., Mahian, O. (2019). Natural convection of hybrid nanofluids inside a partitioned porous cavity for application in solar power plants. *Journal of Thermal Analysis and Calorimetry*, 137(5): 1719-1733. <https://doi.org/10.1007/s10973-019-08019-9>
- [30] Tayebi, T., Öztop, H.F., Chamkha, A.J. (2020). Natural convection and entropy production in hybrid nanofluid filled-annular elliptical cavity with internal heat generation or absorption. *Thermal Science and Engineering Progress*, 19: 100605. <https://doi.org/10.1016/j.tsep.2020.100605>
- [31] Lawrence, J., Alagarsamy, V.K. (2021). Mathematical modelling of MHD natural convection in a linearly heated porous cavity. *Mathematical Modelling of Engineering Problems*, 8(1): 149-157. <https://doi.org/10.18280/mmep.080119>
- [32] Selimefendigil, F., Öztop, H., Abu-Hamdeh, N. (2016). Natural convection and entropy generation in nanofluid filled entrapped trapezoidal cavities under the influence of magnetic field. *Entropy*, 18(2): 43. <https://doi.org/10.3390/e18020043>
- [33] Geridonmez, B.P., Oztop, H.F. (2020). MHD natural convection in a cavity in the presence of cross partial magnetic fields and Al_2O_3 -water nanofluid. *Computers & Mathematics with Applications*, 80(12): 2796-2810. <https://doi.org/10.1016/j.camwa.2020.10.003>
- [34] Marzougui, S., Mebarek-Oudina, F., Assia, A., Magherbi, M., Shah, Z., Ramesh, K. (2020). Entropy generation on magneto-convective flow of copper-water nanofluid in a cavity with chamfers. *Journal of Thermal Analysis and Calorimetry*, 143(3): 2203-2214. <https://doi.org/10.1007/s10973-020-09662-3>
- [35] Al-Farhany, K., Alomari, M.A., Faisal, A.E. (2020). Magnetohydrodynamics mixed convection effects on the open enclosure in a horizontal channel heated partially from the bottom. *IOP Conference Series: Materials Science and Engineering*, 870: 012174. <https://doi.org/10.1088/1757-899x/870/1/012174>
- [36] Selimefendigil, F., Öztop, H.F. (2018). Role of magnetic field and surface corrugation on natural convection in a nanofluid filled 3D trapezoidal cavity. *International Communications in Heat and Mass Transfer*, 95: 182-196. <https://doi.org/10.1016/j.icheatmasstransfer.2018.05.006>
- [37] Ghalambaz, M., Doostani, A., Izadpanahi, E., Chamkha, A.J. (2020). Conjugate natural convection flow of Ag-MgO/water hybrid nanofluid in a square cavity. *Journal of Thermal Analysis and Calorimetry*, 139(3): 2321-2336. <https://doi.org/10.1007/s10973-019-08617-7>
- [38] Hemmat Esfe, M., Abbasian Arani, A.A., Rezaie, M., Yan, W.M., Karimipour, A. (2015). Experimental determination of thermal conductivity and dynamic viscosity of Ag-MgO/water hybrid nanofluid. *International Communications in Heat and Mass Transfer*, 66: 189-195. <https://doi.org/10.1016/j.icheatmasstransfer.2015.06.003>
- [39] Bagheri, H., Behrang, M., Assareh, E., Izadi, M., Sheremet, M.A. (2019). Free convection of hybrid nanofluids in a C-shaped chamber under variable heat flux and magnetic field: Simulation, sensitivity analysis, and artificial neural networks. *Energies*, 12(14): 2807. <https://doi.org/10.3390/en12142807>
- [40] Nasrin, R., Alim, M.A. (2013). Free convective flow of nanofluid having two nanoparticles inside a complicated cavity. *International Journal of Heat and Mass Transfer*, 63: 191-198. <https://doi.org/10.1016/j.ijheatmasstransfer.2013.03.068>
- [41] Abdulkadhim, A., Abed, A.M., Mohsen, A.M., Al-Farhany, K. (2018). Effect of partially thermally active wall on natural convection in porous enclosure. *Mathematical Modelling of Engineering Problems*, 5(4): 395-406. <https://doi.org/10.18280/mmep.050417>

NOMENCLATURE

| | |
|----------|---|
| C_p | Specific heat, J. kg ⁻¹ .K ⁻¹ |
| g | Gravitational acceleration, m.s ⁻² |
| Ha | Hartman number |
| k | Thermal conductivity, W.m ⁻¹ . K ⁻¹ |
| Nu | Nusselt number |
| P | Non-dimensional pressure |
| Pr | Prandtl number |
| Ra | Rayleigh number |
| Rk | Thermal conductivity ratio |
| T | Dimensional temperature, K |
| U | Non-dimensional velocity component X-direction |
| V | Non-dimensional velocity component Y-direction |
| W | Non-dimensional Length of the enclosure |
| X | Non-dimensional X-coordinates |
| Y | Non-dimensional Y-coordinates |
| Θ | dimensionless temperature |
| μ | dynamic viscosity, kg. m ⁻¹ .s ⁻¹ |

Greek symbols

| | |
|----------|---|
| Ψ | Absolute stream function |
| ϕ | Solid volume fraction |
| θ | Dimensionless temperature |
| ρ | density, J.kg ⁻¹ .K ⁻¹ |
| μ | Dynamic viscosity, kg. m ⁻¹ .s ⁻¹ |
| α | Thermal diffusivity, m ² .s ⁻¹ |
| β | Thermal expansion coefficient, K ⁻¹ |

Subscripts

| | |
|-------|--------------------|
| avg | Average |
| c | Cold |
| f | Fluid (pure water) |
| h | Hot |
| L | Local |
| hnf | Hybrid Nanofluid |